Progress In Electromagnetics Research B, Vol. 24, 103–120, 2010

A NEW STRUCTURE OF MMI POLYMER THERMO-OPTIC SWITCH WITH A HIGH REFRACTIVE INDEX CONTRAST

A. M. Al-Hetar †, A. B. Mohammad, and A. S. M. Supa'at

Photonics Technology Center (PTC)
Infocomm Research Alliance (IcRA)
University Technology Malaysia (UTM)
Johor 81310, Malaysia

Z. A. Shamsan

Faculty of Engineering and Information Technology
Communications and Computer Department
Taiz University
Taiz, Yemen

I. Yulianti

Photonics Technology Center (PTC)
Infocomm Research Alliance (IcRA)
University Technology Malaysia (UTM)
Johor 81310, Malaysia

Abstract—The 2 × 2 MMI polymer thermo-optic switch in a high refractive index contrast (0.102) with a new structure design is realized. This device was fabricated using standard fabrication techniques such as coating, photolithography, and dry etching. A crosstalk level of −36.2 dB has been achieved. Meanwhile the extinction ratio of 36.1 dB has been achieved in this device. The polarization dependent loss (PDL) of 0.3 dB and Insertion loss of 1.4 dB were measured at 1550 nm wavelength. In terms of wavelength dependency, the device shows a good performance within C-band wavelength with vacillation of the insertion loss value around 0.88 dB. The power consumption of 1.85 mW was measured to change the state of the switch from the cross to bar state. The measured switching time was 0.7 ms.

Received 22 June 2010, Accepted 29 July 2010, Scheduled 6 August 2010
Corresponding author: A. M. Al-Hetar (alhetar_aziz@yahoo.com).
† Also with Faculty of Engineering and Information Technology, Communications and Computer Department, Taiz University, Taiz, Yemen.

1. INTRODUCTION

There is an increasing need for optical switch matrices for switching, protection switching, cross connection, and dynamic variable optical distribution. It is desirable that such switches have large optical bandwidth, small physical dimensions, large fabrication tolerances, and good performances. These properties are sought in order to reduce optical network system costs and improve efficiency. The conventional integrated optical switches, such as directional coupler switch [1] which is highly sensitive to dimension variation during fabrication and the polarization of optical field, or Y-branch switch [2–4] which requires high electrical power to achieve switch function and has very limited fabrication tolerances. Optical switches based on multimode interference (MMI) couplers, have gained considerable popularity in recent years. MMI couplers have compactness [5–7], relaxed fabrication tolerance, and low wavelength dependent loss (WDL) [8], as well as low polarization dependent loss (PDL) [9, 10] and suitability for device integration [11] which are the subject of interest in high capacity WDM network. All these features make MMI an ideal choice compared to directional couplers or Y-branches.

The MMI switches based on thermo-optic effect are very attractive due to their simplicity and flexibility. Polymer is the most attractive material to fabricate thermo-optic switches for its high thermo-optic coefficient. The thermo-optic effect refers to the variation of the refractive index of a heated dielectric material [12, 13]. The thin-film heater is utilized to change the refractive index and propagation characteristics of the waveguide. The improvement of optical switches performance is crucial to fulfil the requirements of switching, protection switching, cross connection, and dynamic variable optical distribution applications

In this work, a new structure has been used to realize a 2×2 MMI polymer thermo-optic switch. A strongly guiding ridge waveguide with deep etching in the lower cladding has been used. In addition, a ridge silicon is extended from the silicon substrate to the lower cladding and between heater electrodes. The main purpose behind this change in substrate layer is to localize the heating at a heated region and limit the heat diffusion elsewhere [14, 15]. The experimental results show that the 2×2 MMI polymer thermo-optic switch has a low switching power of less than 1.85 mW, a crosstalk at two states of less than -36.2 dB, a switching speed of less than 0.7 ms, an extinction ratio (ER) of higher than 36.1 dB, PDL of less than 0.3 dB at wavelength 1550 nm, and WDL of less than 0.88 dB over C-band.

This paper is organized as follows: in Section 2, the design and

simulation of the 2×2 MMI polymer thermo-optic switch with new structures are presented. The fabrication steps are shown in Section 3. Finally, Section 4 is dedicated to describe the measurements and results.

2. DESIGN AND SIMULATION

In the following simulation, we select the operation wavelength in free space $\lambda = 1550\,\text{nm}$, the core and cladding are ZPU12-480 and LRF378, their refractive indices are 1.48 and 1.378; respectively. ZPU12-480 and LRF378 are photoactive UV curable resins based on perfluorinated acrylate polymers. They have been synthesized at Chemoptics Co. Ltd. in South Korea and used in realizing the device. The electrode is made of aluminum (Al) and the substrate is Si wafer with a refractive index of 3.5.

Figure 1 shows the structural schematic of 2×2 MMI thermo-optic switch which has been proposed with a silicon ridge at substrate layer [14]. The silicon ridge is expanded from silicon substrate layer to the lower cladding layer at the center of MMI coupler and between two self-image areas as shown in Figure 1. It acts as a heat sink [14, 15]. The Strong guiding improves the quality of self images in the MMI section [7]. So the high refractive index contrast (0.102) and a deep etching in the lower cladding are important to improve the quality of self images in the MMI section. The dimensions of the MMI coupler were calculated using the well known relation for general interference in MMI waveguide [10]. The light coupled to the upper input waveguide will be imaged into the lower output waveguide during the cross state (initial state), as shown in Figure 1(a).

In this design, a polarization independent single mode waveguide design is chosen because the polarization dependence in MMI couplers is low [10, 16], and the propagation distance in single mode waveguides

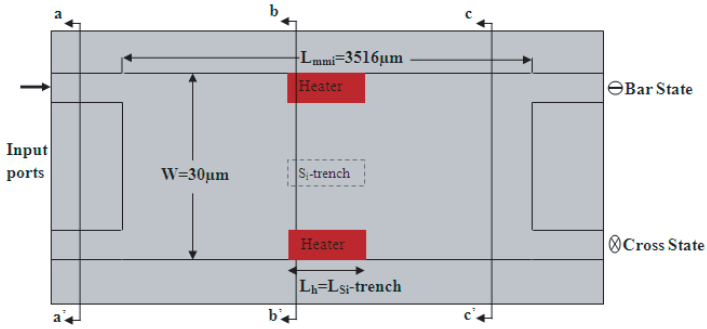

(a)

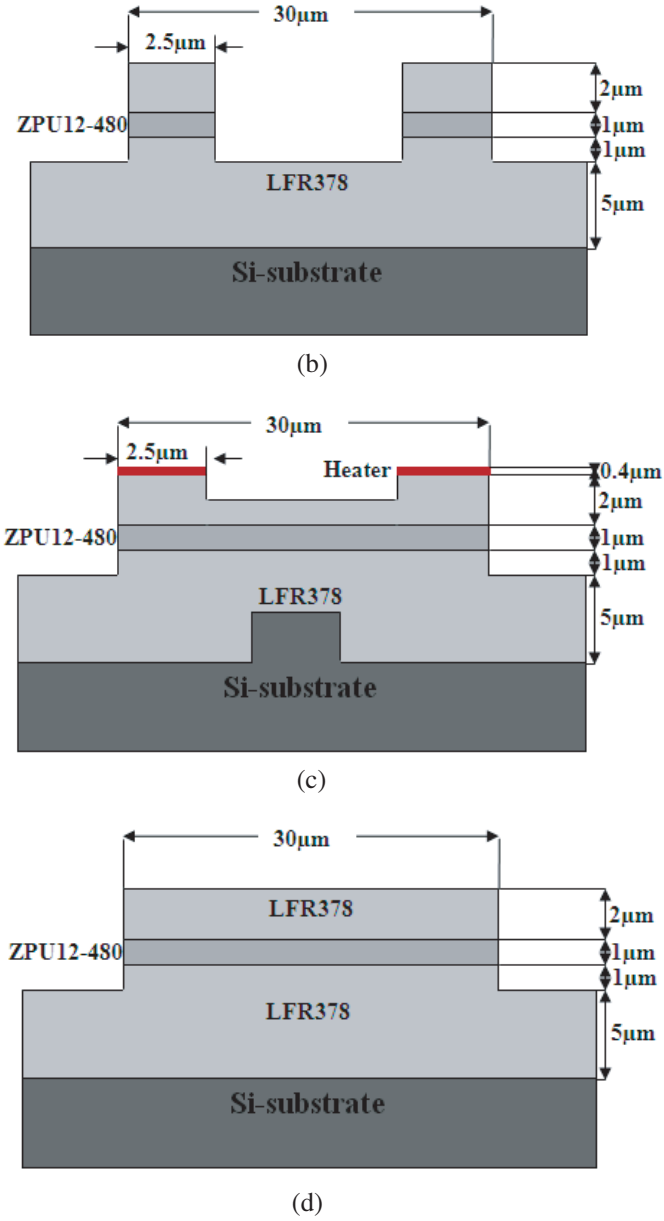

Figure 1. (a) Schematic diagram of the MMI switch, (b) aa' cross section, (c) bb' cross section, and (d) cc' cross section.

is longer. The width and thickness of core layer of access input and output ports have been chosen to ensure single mode and polarization-insensitive propagation in the waveguide. The polarization sensitive of a waveguide is typically characterized by its birefringence, which is the difference of the TE and TM effective refractive indices [17, 18], i.e.,

$$n_{eTE-TM} = n_{eTE} - n_{eTM} \tag{1}$$

Figure 2 shows that the differences of effective refractive indices for the TE and TM modes are nearly identical. The birefringence values has been obtained by calculating the effective TE_0 and TM_0 indices for various waveguide width (W) and thickness (h_{co}) by using 3D Mode Solver BeamPROP, and noting that smallest absolute value of a birefringence occurs at the width of 2.5 μm and thickness of 1 μm, a birefringence is 7×10^{-6}. Typically, symmetric waveguide structures consisting of a square waveguide core surrounded by a uniform cladding region are used to ensure polarization independent propagation [19–21]. While these buried core waveguides achieve polarization independent through symmetry in their geometry, the design in Figure 1(c) uses a combination of geometry, etching and refractive index contrast to achieve the same effect.

The TE and TM single mode field profiles and effective indices have been calculated by using BeamPROP Mode Solver from RSoft. They are shown in Figure 3 for a single mode waveguide width and thickness of 2.5 μm and 1 μm, respectively. The color contours field amplitude values in steps of 10%, while the outermost contour represents 1% field amplitude as shown by scale's figure. The mode fields as shown in Figure 3 are nearly circular in the ridge, which will

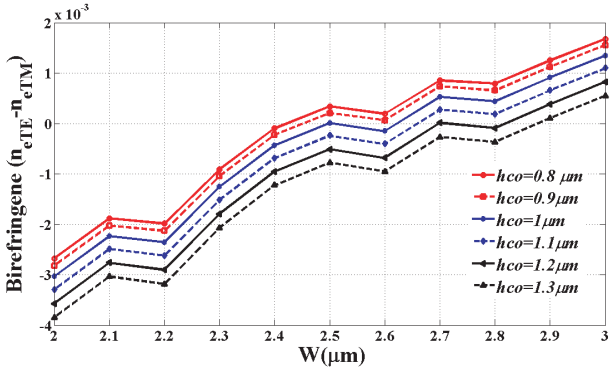

Figure 2. Birefringence (n_{TE}-n_{TM}) in a ridge single mode waveguide for various width (W) and thickness (h_{co}).

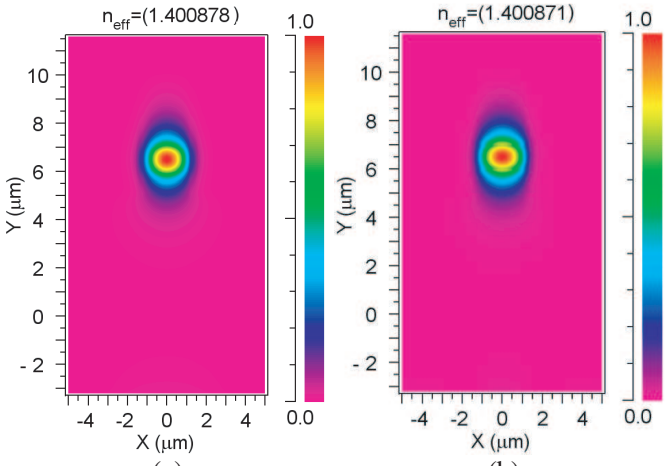

Figure 3. Single mode field profiles for the waveguide structure in Figure 1(c) for (a) TE, and (b) TM.

result in lower coupling losses between the waveguide mode and the circular mode field of an optical fiber.

The key parameter for the operation of the device is that the input light forms a pair of well defined self-images exactly at the middle of switch, and along the central axis of both access waveguides; as shown in Figure 4. In the absence of applied power, light coupled to the first input waveguide is emitted from the second output waveguide, and vice-versa. However, when a π phase shift is applied to either one of the self-images, light coupled to the first input waveguide will be imaged onto the first output waveguide, as shown in Figure 4(b).

The phase shift is controlled by the parameters in Eq. (2) [13, 22].

$$\Delta\phi = k \cdot \Delta n \cdot L_h \tag{2}$$

The phase shift is induced by the change of refractive index n along the tunable section of heater length L_π for a signal with a vacuum wavelength $\lambda = 1550\,\text{nm}$, where $K = 2\pi/\lambda$. The change of refractive index is dependent on the thermal coefficient of material dn/dT and change of temperature ΔT [12].

$$\Delta n = \frac{dn}{dT} \cdot \Delta T \tag{3}$$

The thermal coefficient of ZPU12-480 is $-1.8\times10^{-4}\text{°C}^{-1}$, from Eqs. (2)

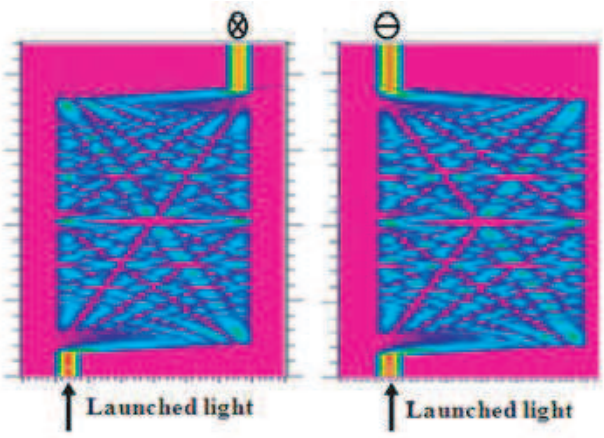

Figure 4. Beam propagation characteristic of MMI switch (a) without index modulation (cross state) and (b) with π phase shift applied to index modulation region (bar state).

and (3) The ΔT in Eq. (4) is sufficient to change phase to π.

$$\Delta T = \frac{4305 \times 10^{-6}}{L_h} \tag{4}$$

The length of self-image inside MMI region is proportional to the width of MMI as shown in Figure 5. Therefore, heater's length should be smaller than or equal to the length of spot image, in case MMI switch which uses the heater inside MMI region to change the phase of image. So the heater's length is restricted with a spot image's length.

Equations (2)–(4) are used to calculate the different temperature (ΔT) which is sufficient to induce a π phase shift in the light traveling through position of spot image. If the length of spot image is small which means that a heater's length is small, a highly different temperature is needed to achieve switching function as shown in Figure 5. Practically, it is impossible to generate high temperature ($T > 280°$C) at heater/upper cladding interface to achieve switching function, since the stability of the material will be affected [23]. Therefore, a wider width is required to increase the length of the heater, and to generate a smaller temperature than previously mentioned to achieve switching functions. According to that, it is important to do trade-off between width of MMI and length of a spot image. The width, $W = 30\,\mu$m is chosen to increase the length of heater ($L_h = 110\,\mu$m) and generate small temperature at heater/upper cladding interface ($T = 108°$C) for optimum working condition.

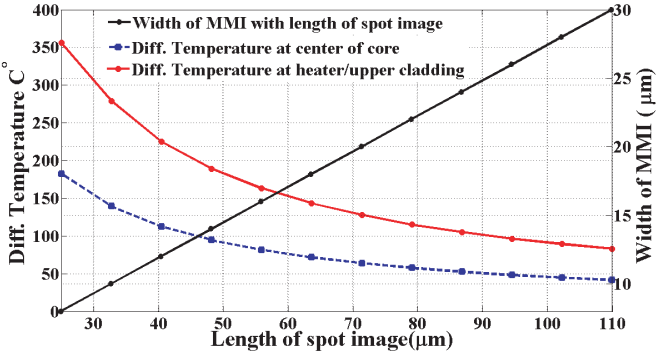

Figure 5. Simulation result for width of MMI with the length of spot image, and length of spot image with a sufficient temperature to achieve switching function.

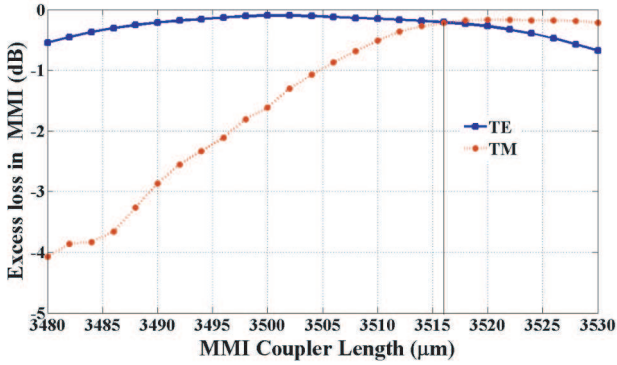

Figure 6. Simulation results for 2×2 MMI coupler, used in the determination of the optimum coupler imaging length.

The performances of 2×2 MMI coupler for various image lengths have been simulated using BeamPROP. The excess losses are found in each length at TE and TM polarization. Results of the simulations for MMI coupler are depicted in Figure 6. Figure 6 clearly shows that there is no single optimum coupler length where excess loss and polarization dependence are minimized. Tradeoffs between the parameters must be made to achieve a suitable image length. The excess losses of TE and TM are almost equal at 3516 µm for MMI coupler's length. To fulfill the lowest PDL in these devices, the final MMI coupler design length is $L_{mmi} = 3516$ µm for MMI switch.

Femlab simulation software from COMSOL is also used. This tool is based on Finite Element Method (FEM) to evaluate the response of heat transfer from the thin-film heater to the structure's layers. The thermal conductivity of Al, Si and polymer (ZPU12-480 and LRF378) are 250 $Wm^{-1\circ}C^{-1}$, 163 $Wm^{-1\circ}C^{-1}$, and 0.2 $Wm^{-1\circ}C^{-1}$ respectively. Figure 7 shows the transient temperature response of the electrode heater and central waveguide of the MMI switch with trench. The rise time (t_{rise}) is defined as the time from 10 to 90% ΔT and the fall time (t_{fall}) is defined as the time from 90% to 10% ΔT. The simulated t_{rise} and t_{fall} are 0.3 ms, which are also the determined switching times for proposed MMI switch.

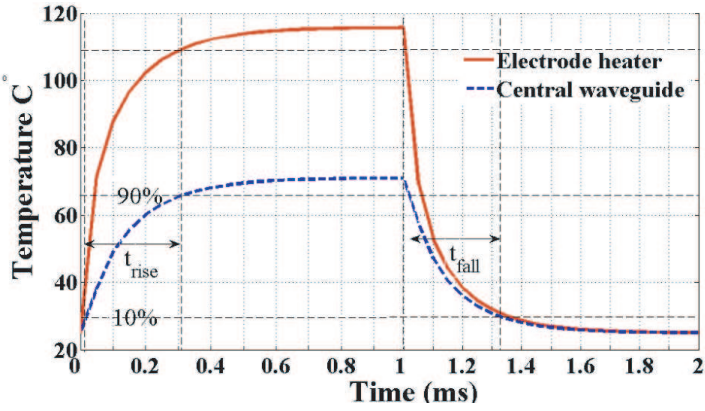

Figure 7. Transient thermal state of the proposed MMI switch.

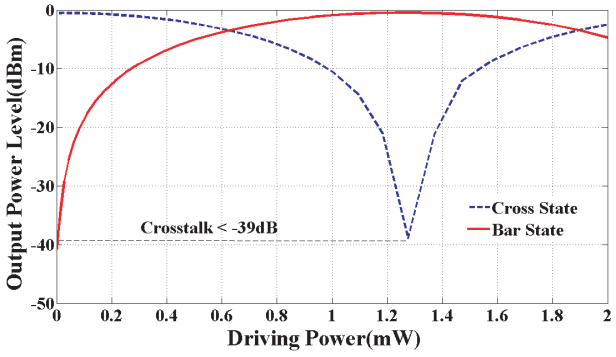

Figure 8. Simulation results based on FD-BPM of channel output versus driving power MMI switch at the cross state and bar state.

The optical and thermal behaviors of proposed 2×2 MMI thermo-optic switch were verified by BeamPROP, it is based on Finite Difference Beam Propagation Method (FD-BPM), and includes the effects of heater. The changing phase is done by certain value of applied power (1.35 mW) as shown in Figure 8. The simulation result shows that the crosstalk (CT) of this structure is -39 dB at the cross state and bar state.

3. FABRICATION

Three different masks have been used in the fabrication process, one for the ridge silicon in substrate layer, one for heater electrodes and heater pads structure, and one for the ridge waveguide structure. The processes involved are depicted in Figure 9.

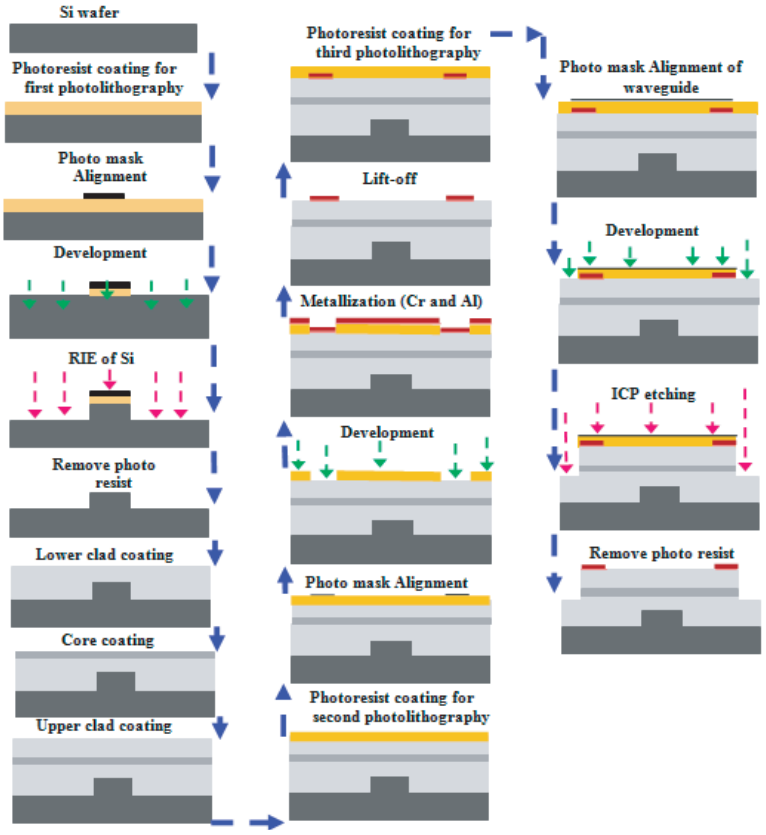

Figure 9. Fabrication steps of polymer thermo-optic switch.

Firstly, a 4-inch Si wafer serves as a substrate which is covered by positive photoresist (Si-PR). After a soft bake (1 minute at 90°C), the ridge Si in substrate is defined through a chromium mask at a wavelength of 410 nm (UV light). After development and a hard bake at 120°C for 30 minutes, the wafer was etched to form a 3 µm ridge height by using Inductively Coupled Plasma Etcher (ICPE). Then LFR378 is spun-coated on the Si substrate as lower cladding. The LFR378 solution was dispensed onto the center of the ridge silicon, approximately 5ml for a 4-inch substrate. Then the substrate was spun at 300 rpm for approximately 3–5 seconds to spread the resin out from the center. The substrate was then spun for 20 seconds at spinning speed 2500 rpm to obtain the desired polymer thickness target at 6 µm. Next, ZPU12-480 is spun-coated on the lower cladding layer. The required thickness of this layer is 1 µm, so the second speed was 3000 rpm for 60 seconds to obtain that thickness. Then, LFR378 is spun-coated on the core layer as upper cladding. The required thickness of this layer is 2 µm. So the second speed was 3000 rpm for 40 seconds to obtain that thickness. After each spinning, the wafer was put in UV chamber for UV curing.

To define the heater electrodes and heater pads, the wafer was covered by negative photoresist (AZ3612) which is the first step in the photolithography. The photoresist thickness must be thicker than the thickness of the Chromium (Cr) (the Cr layer was introduced as an adhesion) and Al. Then, the heater electrodes and heater pads were applied to the negative photoresist. The photoresist layer was patterned in a reverse pattern, i.e., the photoresist layer was removed from the area where the metals are to remain in final structure as shown in Figure 9. Then, the Cr and Al deposition were consecutively done by using e-beam evaporation technique [24] over the masking layer and in openings through the masking layer. The lift-off was performed in a Micrchem Remover PG solution to remove the metals overlying the photoresist layer and leave the desired metal pattern on the underlying surface.

To define the ridge waveguide, the wafer was covered by photoresist which is the first step in the photolithography. Positive photoresist (Si-PR) has been spun at 3500 rpm for 20 seconds to form a layer of photoresist over the wafer. After a soft bake (1 minute at 90°C), the waveguide, heater electrodes, and heaters pads pattern or waveguide pattern was defined through a chromium mask by UV light. After development and a hard bake (30 minutes at 120°C), the wafer was etching to form 4 µm of ridge height by using ICPE.

4. MEASUREMENTS AND DISCUSSION

The experimental setup that was used for all the measurements is shown in Figure 10. The light originated from a tunable laser source (TLS) passed through a polarization controller to choose TE or TM mode and then the light was coupled to the fiber block. The device under test (DUT) was placed on the holder with a vacuum pump and was controlled manually by the rotational stage with XYZ positioning stages. The output light intensity from the DUT was sent to photo diode (PD) and next to the PC. The microprobes were connected to the power supply to drive the electrodes. Additionally, the oscilloscope was connected to the power supply and PD to show the switching response.

The switch curves were investigated by using the experimental setup as shown in Figure 10 which include tunable laser (output level was fixed at 1 mW and wavelength was set to 1550 nm). The relationship between the driving power in mW and the output level power in dBm of each output was measured and shown in Figure 11.

Figure 11 shows the optical power level in the cross port and the bar port responding to the driving power, when the light was launched into P_{i1}. The switch has a crosstalk of -36.2 dB in the cross state (initial state), when there is no driving power to the electrode heater. With driving power increases, the optical power in the cross port decreases but in the bar port will increase simultaneously. Eventually, the switch will reach the bar state (switching state). Here, we define the driven power (applied power to the electrode heater) resulting in maximum optical power in the bar port as the power consumption, which is 1.85 mW, achieving a crosstalk of -36.95 dB. For the fabricated switch, the extinction ratio (ER) is higher than 36.1 dB.

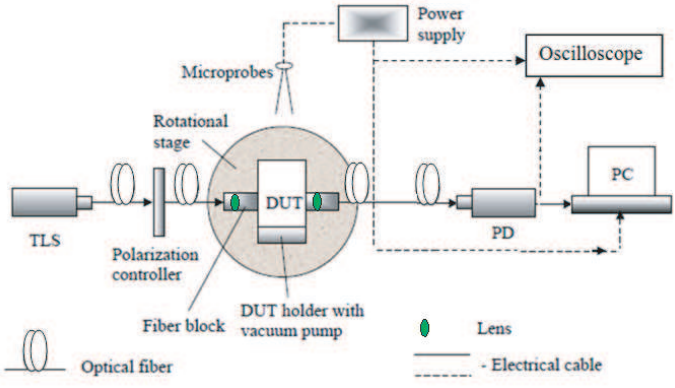

Figure 10. Experimental setup for device characterization.

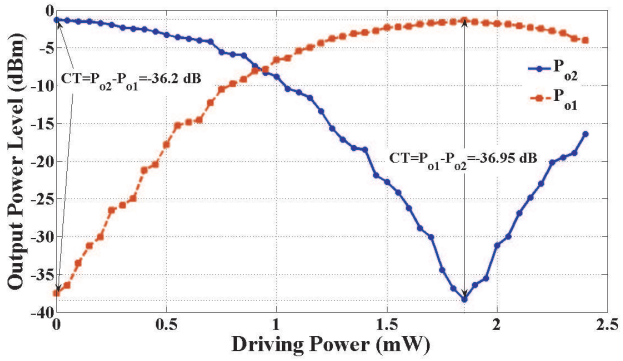

Figure 11. Measured switching curves when light launched into P_{i1}.

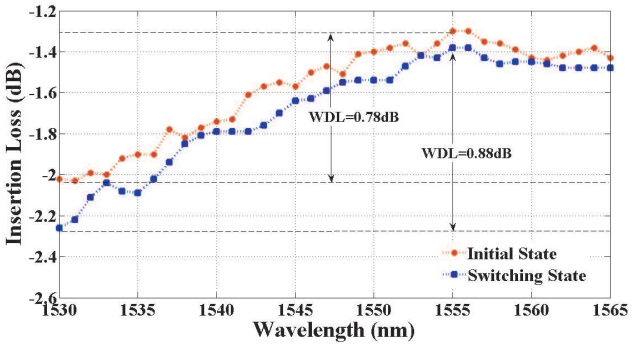

Figure 12. IL as a function of wavelength at initial state and switching state when the light launched to P_{i1}.

Characteristics of the switch within C-band range were done using the same experimental setup shown in Figure 10. The references of the driving power were set at the initial and switching state, which are 0 mW and 1.85 mW, respectively. The results were depicted in Figure 12 when the light was launched into P_{i1}. It can be seen from Figure 12 that wavelength dependent loss (WDL) of the 2×2 MMI optical switch within C-band is 0.78 dB and 0.88 dB at the initial state and switching state respectively when the light was launched to P_{i1}.

The polarization dependent loss (PDL) within C-band range was measured simultaneously. Figure 13 shows the test results when the input is P_{i1} and corresponds to the zero driving power (0 mW) for initial state and 1.85 mW for switching state. It can be seen from Figure 13 that the PDL of the 2×2 MMI optical switch within C-

band is less than 0.54 dB and 0.7 dB at the initial state and switching state respectively when the light was launched to P_{i1}. Same results have been obtained when the input power launched to P_{i2}.

The switching response of the switch is shown in Figure 14. The upper signal is the voltage source which is applied to the electrode heater and the lower signal is the switching response. From Figure 18, the rising (t_{rise}) and falling (t_{fall}) time are 0.3 ms and 0.7 ms, respectively.

Based on theoretical predictions in the simulations, the expected time-power product with optimized electrode is 0.405 mW · ms, while the expected crosstalk is −39 dB. It was found that the switching time of the fabricated device (0.3 ms for t_{rise} and 0.7 ms for t_{fall}) is

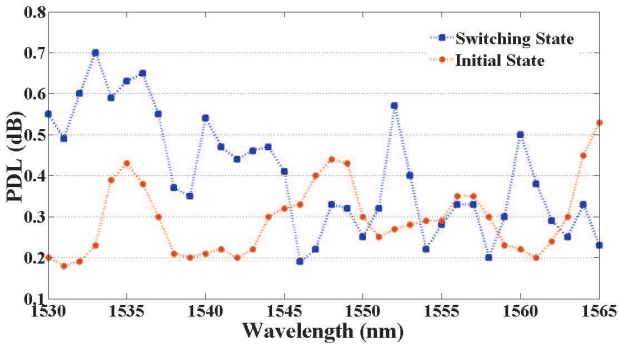

Figure 13. PDL as a function of wavelength at initial state and switching state when the light launched to P_{i1}.

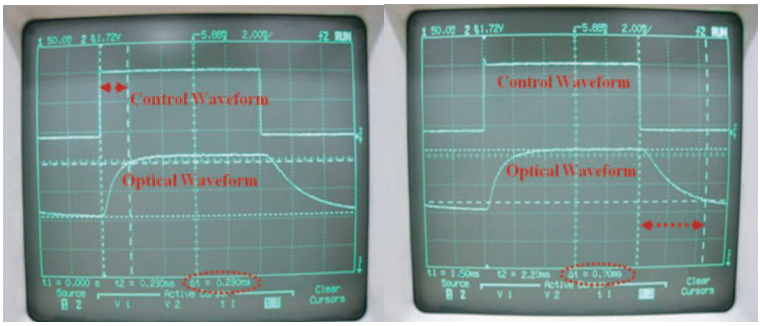

(a) (b)

Figure 14. Dynamic response of the optical signal to the driving signal at (a) rising time, and (b) falling time.

Table 1. Comparison of the performance of the fabricated switch in this work with other published results for polymer based thermo-optic switch.

In × Out	Power-Time product (mW · ms)	CT (dB)	Author
2 × 2	88	−31	[25]
2 × 2	102	−32/−30	[22]
2 × 2	3	−20/−18	[26]
1 × 2	192.4	−23	[27]
2 × 2	1.3	−36.2	Present work

a little slower than the simulation results (0.3 ms for both) especially the cooling time, which is possibly caused by approximation of the 2D-FDTM. In addition, the measured power consumption (1.85 mW) is a little higher than the simulation results (1.35 mW), which is possibly caused by the poor quality of the applied conductive paint connections, resulting in excess power dissipation at the heater contacts. For the 2 × 2 MMI described in this work, the switching time-power product is 1.3 mW · ms. This value is put into perspective by comparison with performance of the polymer based thermo-optic switches published in the literature, given in Table 1. It must be noted that the switch is designed to meet a number of requirements such as that crosstalk, low loss, and polarization insensitivity in addition to the efficient thermo-optic operation, so some of the switches in Table 1 have not been optimized for these later requirements. The fabricated device has the lowest switching time- power product up to date.

Finally, it is the belief then that the good performance of the fabricated device herein is accumulative of materials technology, modified structure, and optimum design. The optical device described herein with these properties is useful for optical path protection, dynamic variable optical power distribution, and optical cross-connect switching.

5. CONCLUSION

The 2 × 2 MMI polymer thermo-optic switch in a high refractive index contrast (0.102) with a new structure design has been realized. This device was fabricated using standard fabrication technique such as coating, photolithography, and dry etching. The optical properties

of the realized device have been measured. The crosstalk level of −36.2 dB for cross state and −36.9 dB for bar state has been achieved. Meanwhile the extinction ratio of 36.1 dB for cross state and 37 dB for bar state has been achieved in this device. The measured Insertion loss and PDL at 1550 nm wavelength were 1.4 dB and 0.3 dB respectively. In terms of wavelength dependency, the device shows a good performance within C-band with vacillation of the insertion loss value around 0.88 dB. The power consumption of 1.85 mW was measured to change the state of the switch from the cross to bar state. While the maximum time to change from the state to the other one was 0.7 ms. The performance of fabricated device is useful for optical path protection, dynamic variable optical power distribution, and optical cross-connect switching.

ACKNOWLEDGMENT

The work of A. M. Al-hetar is supported by the Post-Doctoral fellowship scheme, University Technology Malaysia (UTM) for the project: "Large matrics of optical switching based on multimode interference couplers" under Vot. No. 73519. The authors would like to thank all members of Photonics Technology Centre (PTC) for their cooperation.

REFERENCES

1. Duthie, P. J., N. Shaw, M. Wale, and I. Bennion, "Guided wave switch array using electro-optic and carrier depletion effect in Indium Phosphide," *Electronics Letters*, Vol. 27, No. 19, 1747–1748, 1991.
2. Sneh, A., J. E. Zucker, and B. I. Miller, "Compact low-crosstalk and low propagation loss quantum well Y-branch switches," *IEEE Photonics Technology Letters*, Vol. 8, No. 12, 1644–1646, 1996.
3. Silberberg, Y., P. Perlmutter, and J. E. Baron, "Digital optical switch," *Applied Physics Letters*, Vol. 51, No. 16, 1230–1232, 1987.
4. Ehsan, A. A., S. Shaari, and M. K. Abd-Rahman, "1 × 2 Y-branch plastic optical fiber waveguide coupler for optical access-card system," *Progress In Electromagnetics Research*, Vol. 91, 85–100, 2009.
5. Nagai, S., G. Morishima, H. Inayoshi, and K. Utaka, "Multimode interference photonic switches (MIPS)," *Journal of Lightwave Technology*, Vol. 20, No. 4, 675–680, 2002.

6. Agashe, S. S., K. Shiu, and S. R. Forrest, "Compact polarization-insensitive InGaAsP-InP 2×2 optical switch," *IEEE Photonics Technology Letters*, Vol. 17, No. 1, 52–54, 2005.
7. Shi, Y. and D. Dai, "Design of compact multimode interference coupler based on deeply-etched SiO_2 ridge waveguides," *Optics Communications*, Vol. 271, No. 2, 404–407, 2007.
8. Heaton, J. M., R. M. Jenkins, D. R. Wight, J. T. Parker, J. C. H. Birheck, and K. P. Hilton, "Novel 1-to-N way integrated optical beam splitters using symmetric mode mixing in GaAs/AlGaAs multimode waveguides," *Applied Physics Letters*, Vol. 61, No. 15, 1754–1756, 1992.
9. Besse, P. A., M. Bachmann, H. Melchior, L. B. Soldano, and M. K. Smit, "Optical bandwidth and fabrication tolerances of multimode interference couplers," *Journal of Lightwave Technology*, Vol. 12, No. 6, 1004–1009, 1994.
10. Soldano, L. B. and E. C. M. Pennings, "Optical multi-mode interference devices based on self-imaging: Principles and applications," *Journal of Lightwave Technology*, Vol. 13, No. 4, 615–627, 1995.
11. Jenkins, R. M., J. M. Heaton, D. R. Wight, J. R. Parker, J. C. Birbeck, G. W. Smith, and K. P. Hilton, "Novel $1 \times N$ and $N \times N$ integrated optical switches using self-imaging multimode GaAs/AIGaAs waveguides," *Applied Physics Letters*, Vol. 64, No. 6, 684–686, 1994.
12. Diemeer, M. B. J., "Polymer thermo-optic space switches for optical communications," *Optical Materials*, Vol. 9, 192–200, 1998.
13. Leuthold, J. and C. H. Joyner, "Multimode interference couplers with tunable power splitting ratios," *Journal of Lightwave Technology*, Vol. 19, No. 5, 700–707, 2001.
14. Al-hetar, A. M., I. Yulianti, A. S. M. Supa'at, and A. B. Mohammad, "Thermo-optic multimode interference switches with air and silicon trenches," *Optics Communications*, Vol. 281, 4653–4657, 2008.
15. Al-hetar, A. M., A. S. M. Supa'at, A. B. Mohammad, and I. Yulianti, "Crosstalk improvement of a thermo-optic polymer waveguide MZI–MMI switch," *Optics Communications*, Vol. 281, 5764–5767, 2008.
16. Fujisawa, T. and M. Koshiba, "Theoretical investigation of ultrasmall polarization-insensitive 1×2 multimode interference waveguides based on sandwiched structures," *IEEE Photonics Technology Letters*, Vol. 18, No. 11, 1246–1248, 2006.

17. Kalyanasundaram, N. and P. Muthuchidambaranathan, "Nonlinear pulse propagation in a weakly birefringent optical fiber Part 1: Derivation of coupled nonlinear schrodinger equations (cnlse)," *Progress In Electromagnetics Research B*, Vol. 19, 205–231, 2010.
18. Manning, R. J., A. Antonopoulos, R. L. Roux, and A. E. Kelly, "Experimental measurement of nonlinear polarisation rotation in semiconductor optical amplifiers," *Electronics Letters*, Vol. 37, No. 4, 229–230, 2001.
19. Kawachi, M., "Silica waveguides on silicon and their application to integrated-optic components," *Optical and Quantum Electron*, Vol. 22, No. 5, 391–416, 1990.
20. Lai, Q., W. Hunziker, and H. Melchior, "Low-power compact 2×2 thermooptic silica on- silicon waveguide switch with fast response," *IEEE Photonics Technology Letters*, Vol. 10, No. 5, 681–683, 1998.
21. Supa'at, A. S. M., M. H. Ibrahim, A. B. Mohammad, N. M. Kassim, and E. Ghazali, "A novel thermooptic polymer switch based on directional coupler structure," *American Journal of Applied Sciences*, Vol. 5, No. 11, 1552–1557, 2008.
22. Al-Hetar, A. M., A. S. M. Supa'at, and A. B. Mohammad, "A ridge waveguide for thermo-optic application," *Progress In Electromagnetics Research Letters*, Vol. 6, 1–9, 2009.
23. Ma, H., A. Jen, and L. Dalton, "Polymer-based optical waveguides: Materials, processing, and devices," *Advanced Materials*, Vol. 14, No. 19, 1339–1365. 2002.
24. Cheng, T., G. Drew, B. Gillispie, J. Simko, C. Militello, A. Waldo, and A. Wong, "Vapor deposited thin gold coatings for high temperature electrical contact," *IEEE Proceedings of the 18th International Conference on Electrical Contact*, 404–413, Chicago, IL, USA, September 1996.
25. Wang, F., J. Yang, L. Chen, X. Jiang, and M. Wang, "Optical switch based on multimode interference coupler," *IEEE Photonics Technology Letters*, Vol. 18, No. 2, 421–423, 2006.
26. Gao, L., J. Sun, X. Sun, C. Kang, Y. Yan, and D. Zhang, "Low Switching Power 2×2 thermo-optic switch using direct ultraviolet photolithography process," *Optics Communications*, Vol. 282, 4091–4094, 2009.
27. Yulianti, I., A. S. M. Supa'at, S. M. Idrus, and A. M. Alhetar, "Cosine bend-linear waveguide digital optical switch with parabolic heater," *Optics & Laser Technology*, Vol. 42, 180–185, 2010.